Analytical Design of Small Scale Magnetic Levitation and Propulsion System for Maglev Train Application

Han-Wook Cho
Department of Electric, Electronic and Communication Engineering Edu., Chungnam National University, 99 Daehak-ro, Yuseong-gu, Daejeon, Korea
hwcho@cnu.ac.kr

Chang-Hyun Kim, Jong-Min Lee and Hyung-Suk Han
Department of Magnetic Levitation and Linear Drive, Korea Institute of Machinery and Materials, 104 Sinseong-ro, Yuseong-gu, Daejeon, Korea
chkim78@kimm.re.kr , lee_jm@kimm.re.kr , hshan@kimm.re.kr

ABSTRACT: This paper deals with the design and characteristic analysis of small scale magnetic levitation and propulsion system for maglev train application. A magnetic circuit model and its results were derived for the levitation and propulsion magnets. Also, we verified it by comparing the experiments with simulation.

1 INTRODUCTION

Electromagnetically levitated and guided systems are commonly used in the field of people transport vehicles, tool machines and conveyor system because of its silent and non-contacted motion [1][2]. In this paper, a solution with practical result is presented based on a manufactured small scale magnetic levitation and propulsion system. We analyzed the characteristics of linear synchronous motor (LSM) containing electromagnets. The geometry of the LSM is characterized by hybrid-excitation, which combines the high-energy density of permanent magnets and the controllability of easily implemented electrical excitation. The electromagnet with permanent magnet has several advantages such as an increased levitation airgap height, a decrease in the total weight of the vehicle, and a large improvement in thermal conditions [3]-[5].

The effective electric-gap of a maglev system is relatively large; the gap includes the height of the permanent magnet with the permeability of air and a large slot for the stator. Moreover, because the device is a three-dimensional (3-D) model and the leakage flux shows complex behavior, a detailed investigation involving 3-D electromagnetic field calculations are required.

Fig 1. Concept of high-speed maglev.

The aim of this study is to investigate the force characteristics of a small scale magnetic levitation and propulsion system. The feasibility of the electromagnets and linear motor for maglev vehicles is confirmed by testing the levitation force.

2 MAGNETIC CIRCUIT ANALYSIS OF SMALL SCALE MAGNETIC LEVITATION AND PROPULSION SYSTEM

A. Magnetic Levitation and Propulsion System

The development concept of the high-speed magnetic levitation and propulsion system is shown in Fig.1. The electromagnets are located on each side of the vehicle. Each of electromagnets contained a permanent magnet that generated a nominal magnetic flux for the required levitation force and a coil that

perturbed the magnetic flux and varied the magnetic force to adjust the airgap length. There are slots and coils for linear generator on the top of the core. Long-stator LSM core and windings are arranged along the double-side track.

Table I lists the specifications and design parameters of the small scale magnetic levitation and propulsion system.

TABLE I
Specification and Small Scale Maglev System

Translator Part		Long-Stator Part	
Item	Value	Item	Value
Pole Pitch	78 mm	Slot Pitch	52 mm
N. of Poles	12	Slots/Poles	3/2
Stack Length	50 mm	Nom. Airgap	3 mm
Initial Airgap	5 mm	Min. Airgap	1 mm

B. Unit Magnet with Aligned Position

Fig. 2 shows the design parameters of unit module of small scale magnetic levitation electromagnets at aligned position.

The permanent magnet was made from neodymium-iron-boron alloy and provides the nominal magnetic flux for the levitation force. The magnetic forces could be calculated analytically using magnetic circuit instead of numerical methods such as the finite element method. However, the leakage of the flux and the fringing field around the corner of the iron cores in air should be considered to obtain more accurate results. The magnetic fluxes around the magnet were assumed as illustrated in Fig.2. Fig 2(a) and (b) shows the design parameters and respective reluctances of small scale magnetic levitation and propulsion system as well.

Fig 3 shows the magnetic circuit and respective electromagnetic symbols of unit magnet with aligned position. Fig.4 shows the equivalent magnetic circuit model of unit magnet with aligned position. It has the permanent magnet field only.

In the equivalent magnetic circuit, the permanent magnet can be modeled with coercieve force F_c :

$$F_c = R_m \Phi_r = \frac{B_r l_{pm}}{\mu_0 \mu_r} \qquad (1)$$

where, B_r is the residual flux or remanent flux of permanent magnet. R_{sc} and R_{tc} is the stator and translator core reluctance. Rlt and Rfg mean the leakage and fringing flux path reluctances in the stator translator core parts.

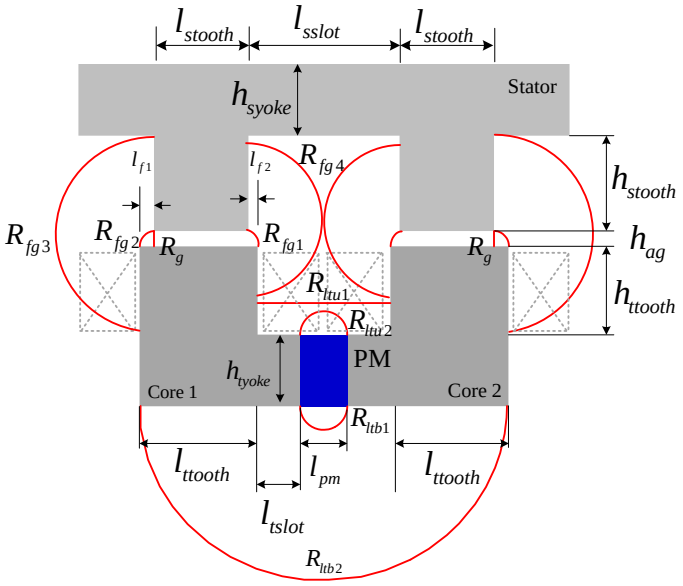

(a)

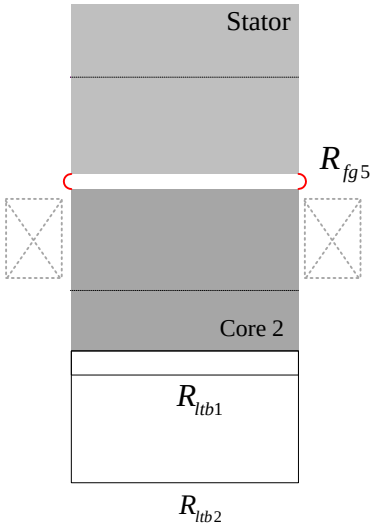

(b)

Fig. 2. Magnetic fluxes and respective reluctances of the levitation magnet with aligned position. (a) side view, (b) front view

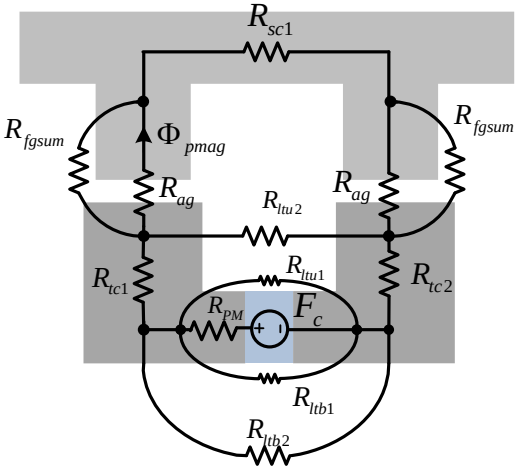

Fig. 3. Magnetic circuit and electromagnetic symbols of unit magnet with permanent magnet only.

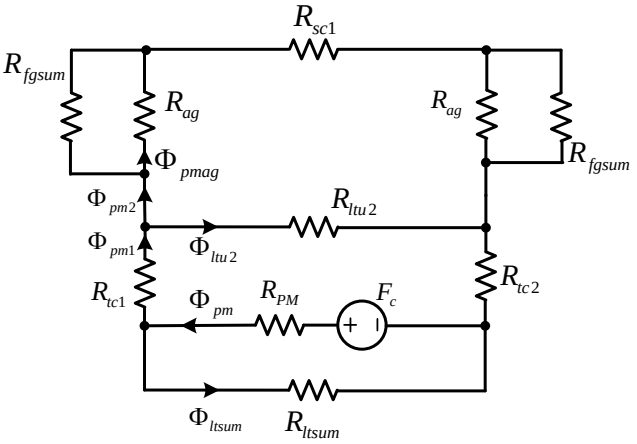

Fig. 4. Equivalent magnetic circuit model of unit magnet with aligned position – Permanent magnet field only.

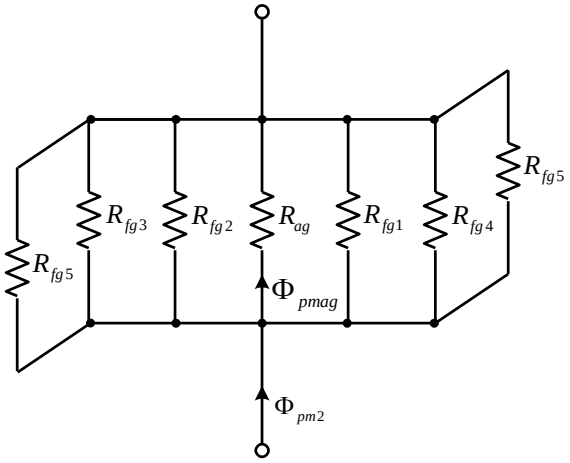

Fig. 5. Airgap and friging path fluxes and respective reluctances at the airgap region.

Fig 5 illustrates the airgap and fringing path fluxes and respective reluctances at the airgap region. The magnetic flux by permanent magnet can be calculated by :

$$\Phi_{pmag} = \frac{P_{fgsum}}{R_{fgsum} + P_{ag}} \cdot \Phi_{pm2} \tag{2}$$

where,

$$\Phi_{pm} = \frac{P_{ltsum} + P_{sum1}}{P_{pm} + P_{ltsum} + P_{sum1}} \cdot \Phi_r \tag{3}$$

$$\Phi_{pm2} = \frac{P_{sum1}}{P_{ltsum} + P_{sum1}} \cdot \Phi_{pm} \tag{4}$$

$$R_{fgsum} = \frac{1}{\frac{1}{R_{fg1}} + \frac{1}{R_{fg2}} + \frac{1}{R_{fg3}} + \frac{1}{R_{fg4}} + 2 \cdot \frac{1}{R_{fg5}}} \tag{5}$$

where, P_{sum}s are partial sum of reluctances in the equivalent magnetic circuit.

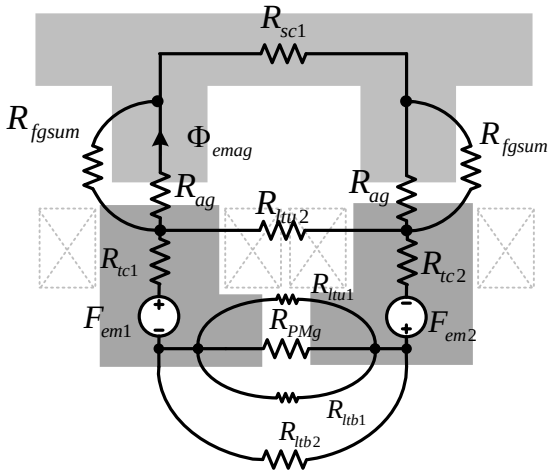

Fig. 6. Magnetic circuit and electromagnetic symbols of unit magnet with electromagnet only.

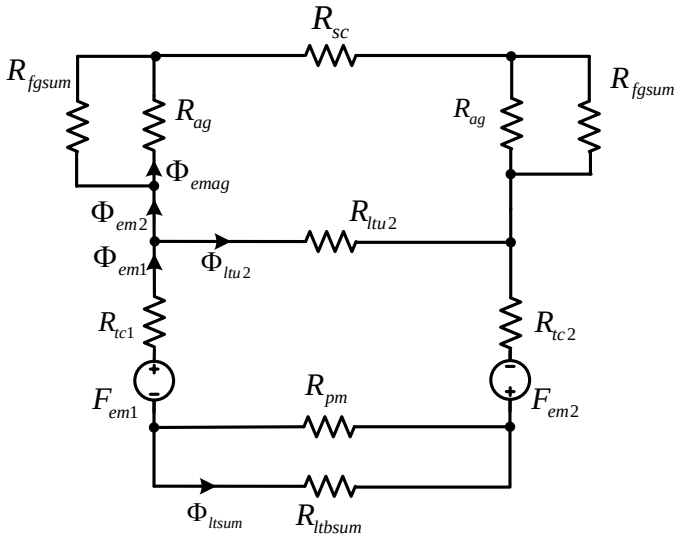

Fig. 7. Equivalent magnetic circuit model of unit magnet with aligned position – electromagnetic magnet field only.

Fig 6 shows the magnetic circuit and respective electromagnetic symbols of unit magnet with electromagnet. Fig.7 shows the equivalent magnetic circuit model of unit magnet with aligned position. It has the electromagnet field only.

In Fig 6, the magneto motive force F_{em1} and F_{em2} can be expressed as following:

$$F_{em1} = F_{em2} = N_{turns} I_{dc} \tag{6}$$

where, N_{turns} is the number of coil turns per pole and I_{dc} is the input control current.

$$\Phi_{em1} = \frac{2N_{turns} I_{dc}}{R_{sum2} + R_{sum3}} \tag{7}$$

$$\Phi_{em2} = \frac{R_{ltu2}}{R_{sum1} + R_{ltu2}} \cdot \Phi_{em1} \tag{8}$$

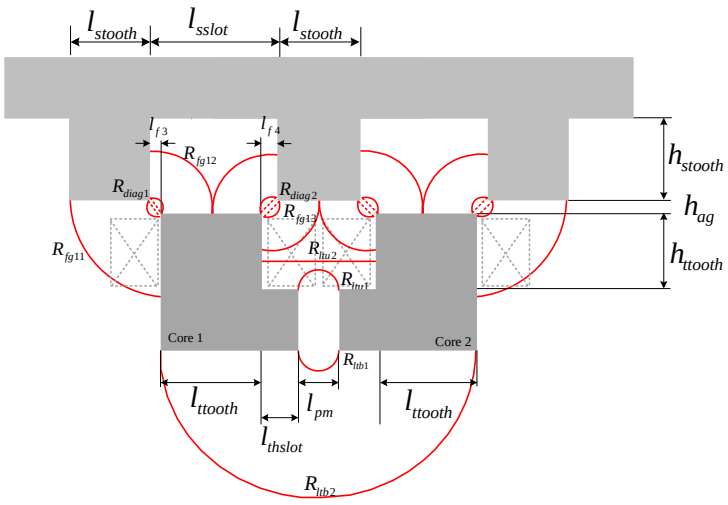

Fig. 8. Magnetic fluxes and respective reluctances of the levitation magnet with unaligned potion.

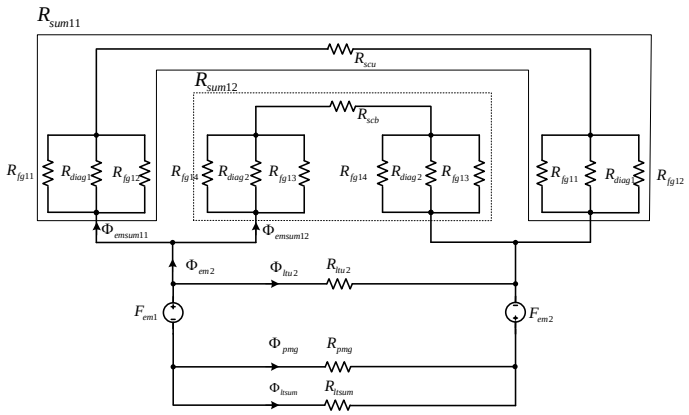

Fig. 9. Equivalent magnetic circuit model of unit magnet with unaligned position – electromagnetic magnet field only.

C. Unit Magnet with unaligned Position

Fig. 8 shows the design parameters of unit module of small scale magnetic levitation electromagnets at unaligned position. Fig.9 shows the equivalent magnetic circuit model of unit magnet with unaligned position. It has the electromagnet field only also.

In Fig 9, the magnetic fluxes cab be expressed as :

$$\Phi_{pm2} = \frac{P_{sum11} + P_{sum12}}{P_{sum11} + P_{sum12} + P_{ltsum} + P_{pm}} \cdot \Phi_r \qquad (9)$$

$$\Phi_{pm\_sum11} = \frac{R_{sum12}}{R_{sum11} + R_{sum12}} \cdot \Phi_{pm2} \qquad (10)$$

$$\Phi_{pm\_sum12} = \frac{R_{sum11}}{R_{sum11} + R_{sum12}} \cdot \Phi_{pm2} \qquad (11)$$

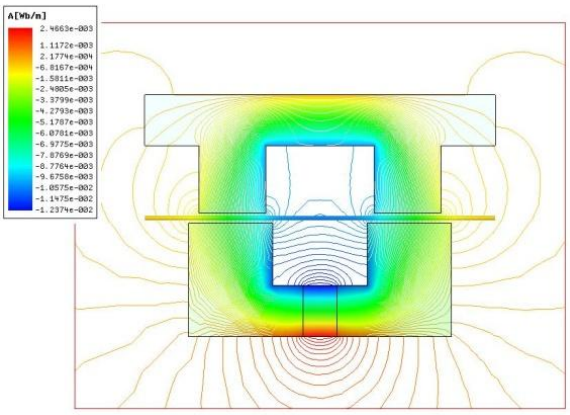

Fig. 10. Magnetic flux distributions of unit module of electromagnet at aligned position.

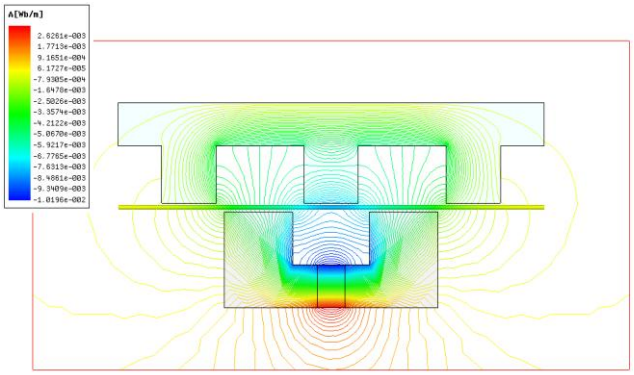

Fig. 11. Magnetic flux distributions of unit module of electromagnet at aligned position.

3 FINITE ELEMENT ANALYSIS

A. Unit Magnet Model

In order to evaluate the basic characteristics of the small scale magnetic levitation and propulsion system, the finite element method is used to analyze both magnetic field distributions and static forces.

Fig 10 and 11 shows the magnetic flux distribution of unit module of electromagnet at aligned position and unaligned position, respectively. As can be seen in the flux distributions, as in Fig. 10 and 15, the airgap flux density exhibits distinct features for each topology.

Figs. 12 and 13 show the comparison of the airgap magnetic flux density of the unit electromagnet at aligned position with airgap 3mm and input current 0, 5 A condition. It can be seen that considering the fringing fluxes improves the accuracy of the developed analytical model. Figs 14 and 15 show the comparison of the airgap magnetic flux density of the unit electromagnet at unaligned position predicted by

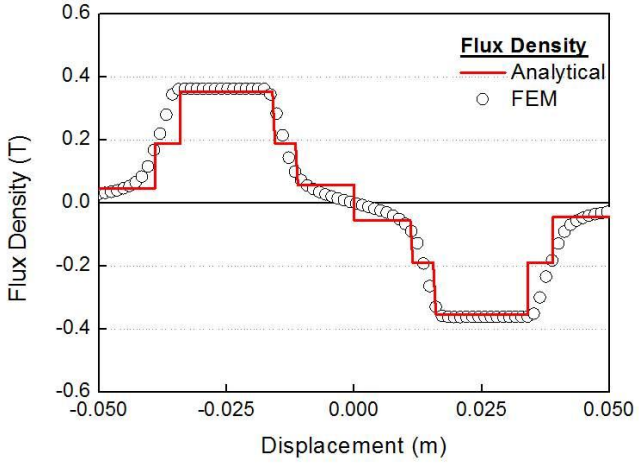

Fig. 12. Comparison of the airgap magnetic flux density of unit electromagnet at aligned position. (airgap 3 mm, current 0A)

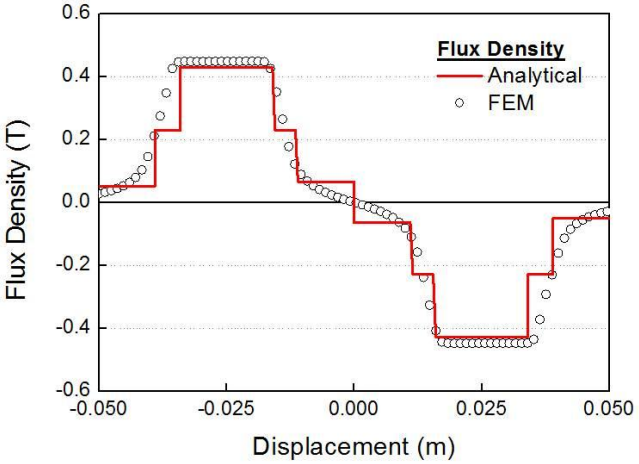

Fig. 13. Comparison of the airgap magnetic flux density of unit electromagnet at aligned position. (airgap 3 mm, current 5A)

analytical and FE analyses. As can be seen, overall, the analytical predictions with due account of the fringing and the leakage effect agree well with the nonlinear FE analysis.

B. Full Magnet 3D Model

Fig. 16 shows the full FE model for the small scale magnetic levitation and propulsion system. In the long stator on the ground, large slots were designed to allow the installation of concentrated copper windings. This device stabilized by an attractive force produced by strong permanent amgnets, which are mounted on the translator core. In order to achieve stable levitation, the permanent magnet's flux must be modulated by the DC-excitation coil surrounding the permanent magnets.

Fig. 17 and 18 show the magnetic flux vector distribution in the long stator and translator cores when there is no armature current and no DC-excitation current for an airgap height of 3 mm.

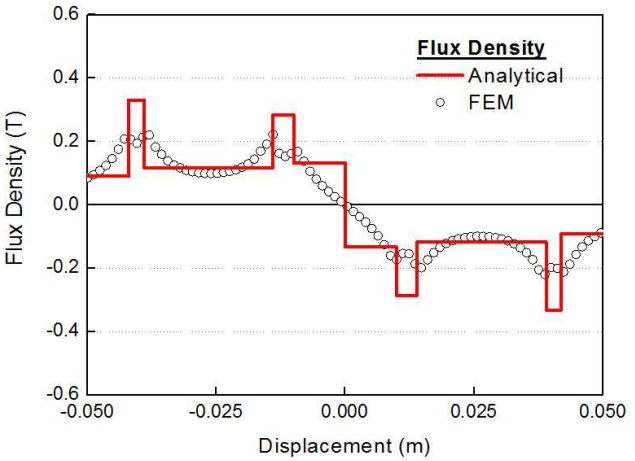

Fig. 14. Comparison of the airgap magnetic flux density of unit electromagnet at unaligned position. (airgap 3 mm, current 0A)

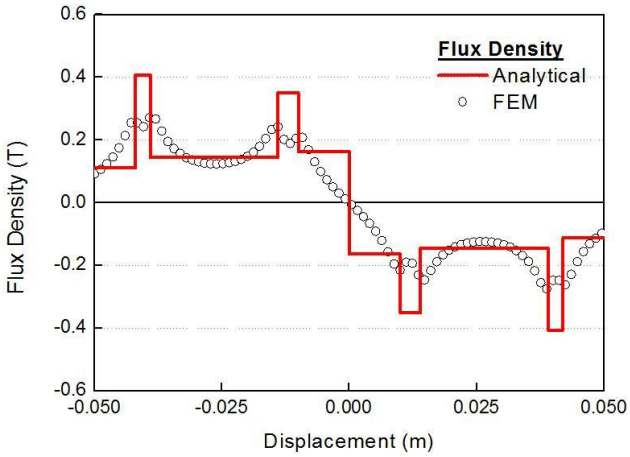

Fig. 15. Comparison of the airgap magnetic flux density of unit electromagnet at unaligned position. (airgap 3 mm, current 5A)

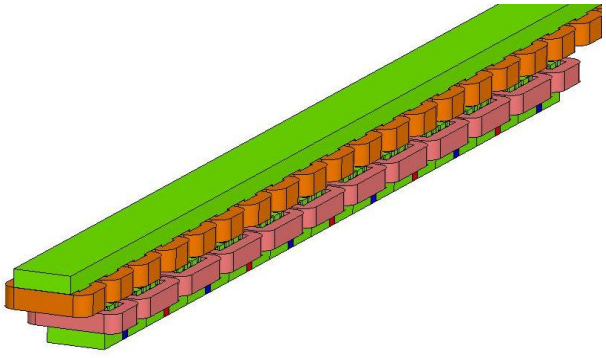

Fig. 16. Magnetic full FE model for the small scale magnetic levitation and propulsion system.

There is a large leakage flux linking with the translator cor in the lateral edge region.

Fig. 19 shows the comparison of the airgap magnetic flux density of full electromagnet of the small scale magnetic levitation and propulsion system. As can be seen, overall, the analytical

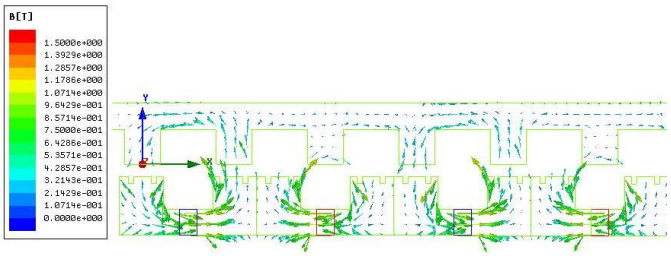

Fig. 17. Magnetic fluxes and respective reluctances of the levitation magnet.

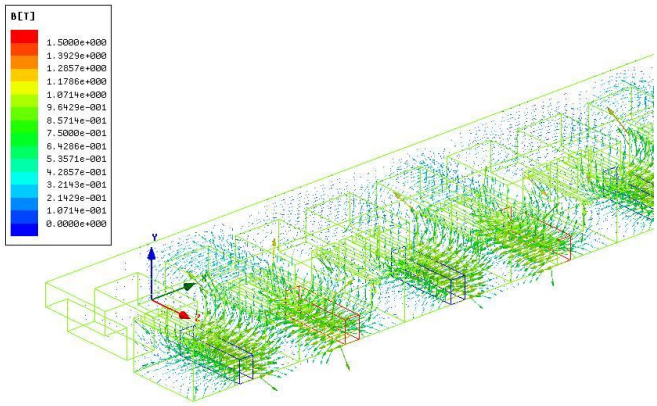

Fig. 18. Magnetic fluxes and respective reluctances of the levitation magnet.

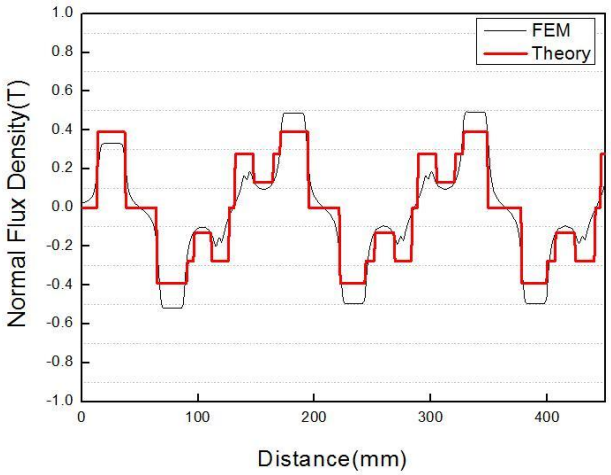

Fig. 19. Comparison of the airgap magnetic flux density of full electromagnet of the small scale magnetic levitation and propulsion system.

predictions agree well with the nonlinear FE analysis in the full electromagnet as well.

Table II lists the comparison of the force characteristics predicted by analytical and FE analysis. It can be seen that the error between FE and analytical predictions being $\leq$22.6%.

Fig. 20 shows the levitation force as a function of the airgap length and input DC-excitation current. It can be seen that the rated airgap is 3 mm for a rated load of 166.3 kg at zero current. In addition, the

TABLE II
Comparison of the Force Characteristics Predicted by Analytical and FE Analysis

	EMC	FEM	Error
Attraction Force	1150	1485	22.6

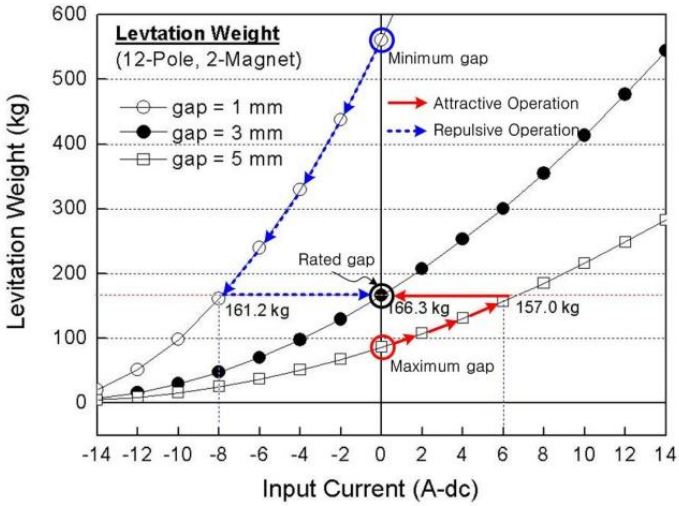

Fig. 20. Levitation force vs. input current as a parameter of airgap.

figure shows the limit wieght of vehicle part including translator.

4 EXPERIMENT

In order to experimentally validate the forgoing analyses, the small scale magnetic levitation and propulsion system has been manufactured. Fig. 21 shows the long-stator core, the translator core ,and the assembled small scale magnetic levitation and propulsion system.

The developed small scale magnetic levitation and propulsion system is shown in Fig.22.

Fig. 23 and 24 shows the transient responses of airgap length and electromagnet coil current at the front and rear electromagnets on the vehicle. These results shows that electro-magnet coil current of instantaneous magnitude about +2.2 A~ 2.5 A and levitation gap varies from 5 mm to 4 mm. As a result of experiment, it becomes clear that the levitation controller has good response characteristics.

(a)

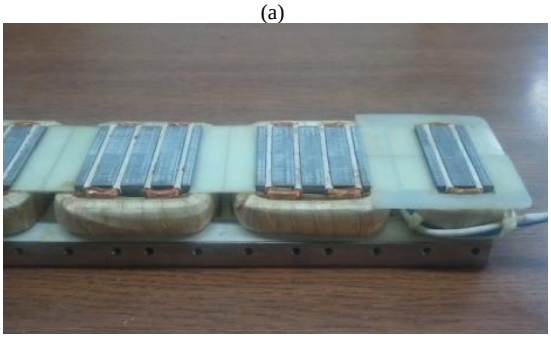

(b)

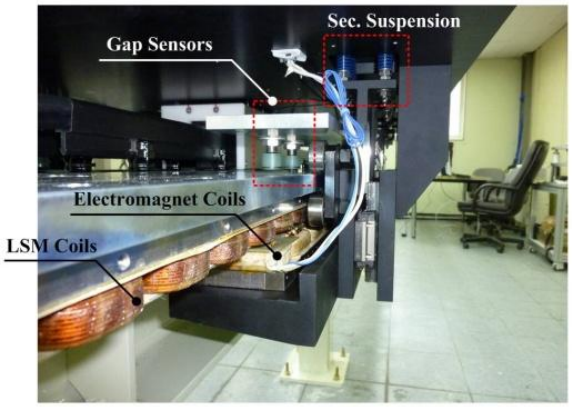

(c)

Fig. 21. Manufactured small scale magnetic levitation and propulsion system. (a) long stator, (b) translator, and (c) assembled vehicle.

Fig. 22. Manufactured small scale magnetic levitation and propulsion system.

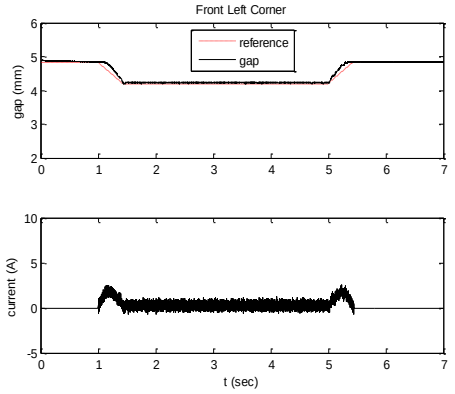

(a)

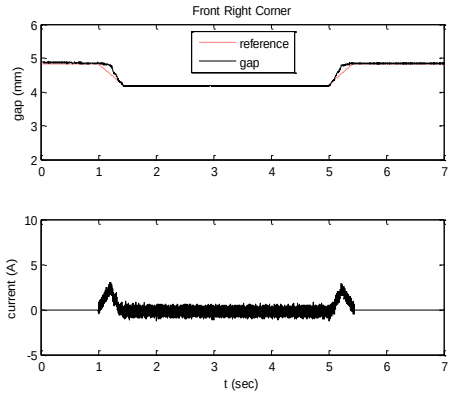

(b)

Fig. 23. Levitation characteristics (a) front-left corner, (b) front right corner.

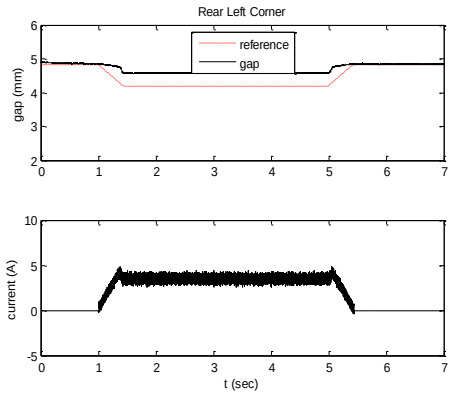

(c)

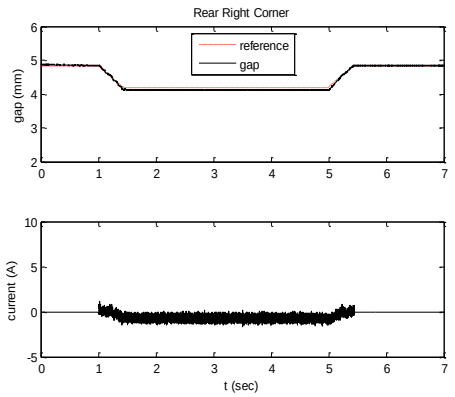

(d)

Fig. 24. Levitation characteristics (a) rear-left corner, (b) rear-right corner.

5 CONCLUSION

By utilizing simple lumped magnetic circuit models, the force characteristics of electromagnet of the small scale magnetic levitation and propulsion system can be calculated analytically. Although the models are simple, they can account for the fringing and leakage effect. In addition, we manufacture an experimental system and tested for the levitation and propulsion system. Experiments are now being conducted to get more useful data.

ACKNOWLEDGMENT

This work was supported by Royalty Project through Korea Institute of Construction & Transportation Technology Evaluation and Planning(KICTEP) funded by Korean Ministry of Land, Transport and Maritime Affairs(10ENGF-C055954-01-000000)

6 REFERENCES

Aldo D'Arrigo, Alfred Rufer, "Integrated electromagnetic levitation and guidance system for the swissmetro project," MAGLEV 2000, Rio de Janeiro, Brazil, pp.263-268, 2000.

Y.J.Kim, P.S.Shin, D.H.Kang, and Y.H.Cho, "Design and analysis of electromagnetic system in a magnetically levitated vehicle, KOMAG-01," *IEEE Transactions on Magnetics*, Vol. 28, No. 5, pp. 3321-3323, September 1992.

M. Morishita, T. Azukizawa, S. Kanda, N. Tamura, and T. Yokoyama, "A new maglev system for magnetically levitated carrier system," *IEEE Trans. Vehicular Tech*., vol. 38, no. 4, pp. 230-236, 1989.

Takashi Onuki, and Tasushi Toda, "Optimal design of hybrid magnet in maglev system with both permanent and electro magnets," *IEEE Trans. Magn*., vol. 29, no. 2, pp. 1783-1786, March 1993.

Yumei Du, Liming Shi, and Nengqiang Jin, "Analysis of the three-dimension forces in a hybrid maglev vehicle system," *Proc. of ICEMS 2003*, pp. 563-565.